Developmental Cell
Article

Ankrd11 Is a Chromatin Regulator Involved in Autism that Is Essential for Neural Development

Denis Gallagher,[1,3,10] Anastassia Voronova,[1,10] Mark A. Zander,[1] Gonzalo I. Cancino,[1] Alexa Bramall,[1] Matthew P. Krause,[1] Clemer Abad,[4] Mustafa Tekin,[4] Paul M. Neilsen,[5] David F. Callen,[6] Stephen W. Scherer,[2,7] Gordon M. Keller,[3,8] David R. Kaplan,[1,7,*] Katherina Walz,[4] and Freda D. Miller[1,3,7,9,*]
[1]Program in Neuroscience and Mental Health
[2]Program in Genetics and Genome Biology
Hospital for Sick Children, Toronto, ON M5G 1L7, Canada
[3]McEwen Center for Regenerative Medicine, University Health Network, Toronto, ON M5G 1L7, Canada
[4]Dr. John T. Macdonald Foundation Department of Human Genetics and John P. Hussman Institute for Human Genomics, Miller School of Medicine, University of Miami, Miami, FL 33136, USA
[5]Swinburne University of Technology, Sarawak Campus, Kuching 93350, Sarawak, Malaysia
[6]Centre for Personalised Cancer Medicine, University of Adelaide, Adelaide SA 5000, Australia
[7]Department of Molecular Genetics
[8]Department of Medical Biophysics
[9]Department of Physiology
University of Toronto, Toronto, ON M5G 1X5, Canada
[10]Co-first author
*Correspondence: dkaplan@sickkids.ca (D.R.K.), fredam@sickkids.ca (F.D.M.)
http://dx.doi.org/10.1016/j.devcel.2014.11.031

SUMMARY

Ankrd11 is a potential chromatin regulator implicated in neural development and autism spectrum disorder (ASD) with no known function in the brain. Here, we show that knockdown of *Ankrd11* in developing murine or human cortical neural precursors caused decreased proliferation, reduced neurogenesis, and aberrant neuronal positioning. Similar cellular phenotypes and aberrant ASD-like behaviors were observed in Yoda mice carrying a point mutation in the *Ankrd11* HDAC-binding domain. Consistent with a role for Ankrd11 in histone acetylation, Ankrd11 was associated with chromatin and colocalized with HDAC3, and expression and histone acetylation of Ankrd11 target genes were altered in Yoda neural precursors. Moreover, the *Ankrd11* knockdown-mediated decrease in precursor proliferation was rescued by inhibiting histone acetyltransferase activity or expressing HDAC3. Thus, Ankrd11 is a crucial chromatin regulator that controls histone acetylation and gene expression during neural development, thereby providing a likely explanation for its association with cognitive dysfunction and ASD.

INTRODUCTION

We currently understand little about mechanisms that are dysregulated in human neurodevelopmental disorders like ASD. In ASD, many different genes are affected by sporadic or rare-inherited DNA sequence mutations or copy-number variations (Devlin and Scherer, 2012). Many of these are involved in synapse function, but others, such as Ankyrin repeat domain containing protein 11 (Ankrd11; Zhang et al., 2004), are associated with transcription or chromatin regulation, but have no known role in the brain (Pinto et al., 2014; Iossifov et al., 2014). In humans, deletion or mutation of one allele of the *ANKRD11* gene causes cognitive dysfunction and ASD (Marshall et al., 2008; Sirmaci et al., 2011; Lo-Castro et al., 2013), and some individuals display corpus callosum hypoplasia and periventricular heterotopias (Willemsen et al., 2010). Intriguingly, cell line studies indicate that Ankrd11 is a large nuclear protein that regulates transcription, potentially by binding chromatin modifying enzymes like histone deacetylases (HDACs) (Zhang et al., 2004, 2007a, 2007b; Li et al., 2008; Neilsen et al., 2008).

Modification of chromatin structure by histone acetylation is essential for nervous system development and function and plays a particularly important role in neural precursors (Lilja et al., 2013; Rudenko and Tsai 2014; Castelo-Branco et al., 2014). For example, haploinsufficiency for *CBP* causes cognitive dysfunction in part because it regulates neural precursor development via its histone acetyltransferase (HAT) activity (Wang et al., 2010). HDAC inhibitors and neural-specific knockouts of HDACs 1 and 2 also perturb neural precursor proliferation and differentiation (Lilja et al., 2013), and NCoR, a nuclear coregulator that binds HDACs, is essential for appropriate neural precursor differentiation (Castelo-Branco et al., 2014).

Here, we show that Ankrd11 functions as a nuclear coregulator in the developing brain, regulating histone acetylation and gene expression, and in so doing determining precursor proliferation, neurogenesis, and neuronal positioning. Moreover, we show that when Ankrd11 is decreased or mutated in mice, this perturbs neural development and when mutated, causes aberrant behavior. These findings therefore provide an explanation for the cognitive dysfunction observed when the *ANKRD11* gene is mutated or deleted in humans.

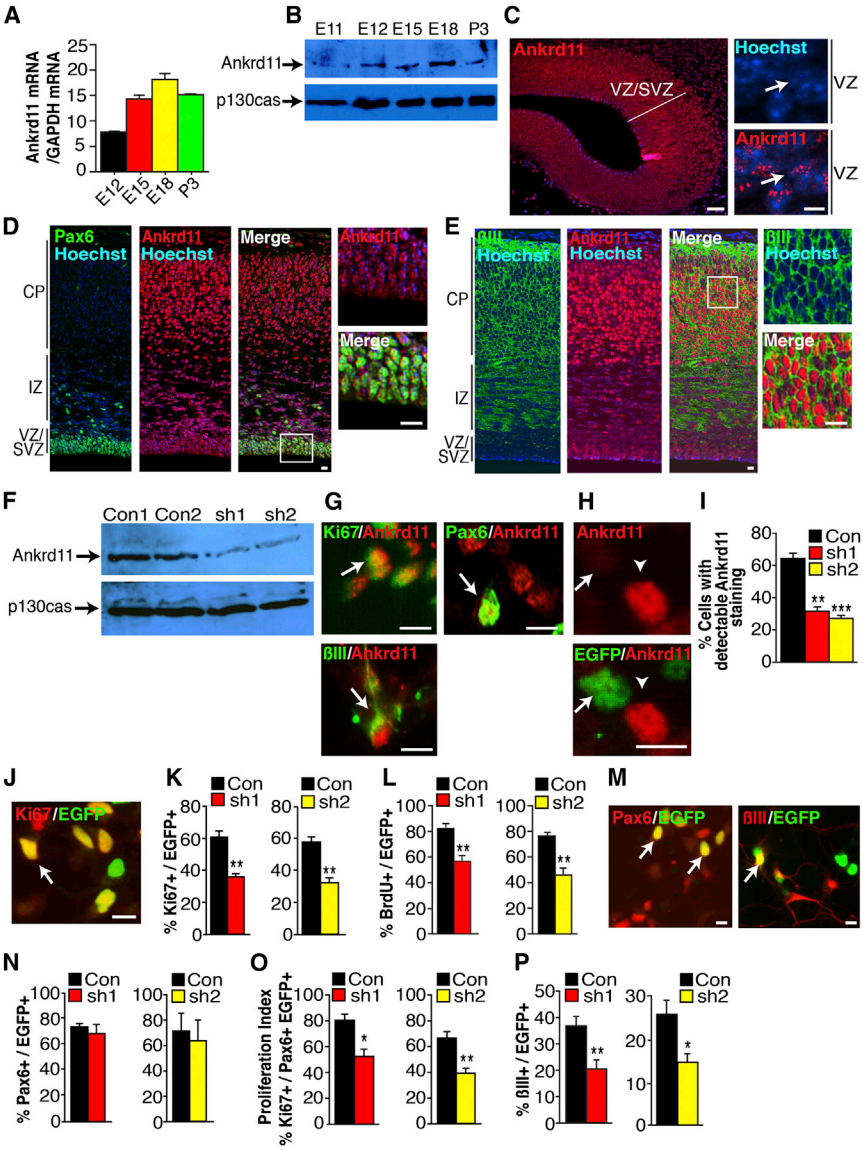

Figure 1. Ankrd11 Is Expressed in Murine Embryonic Cortical Precursors and Regulates Their Proliferation and Differentiation in Culture

(A) Quantitative RT-PCR for *Ankrd11* mRNA relative to *GAPDH* mRNA in the E12 to P3 cortex.

(B) Western blot of Ankrd11 in E11 to P3 cortex. The blot was reprobed for p130cas as a loading control.

(C–E) Images of E12 (C) or E16 (D and E) cortical sections immunostained for Ankrd11 (red) and Pax6 (D, green) or βIII-tubulin (E, green) and counterstained with Hoechst 33258 (blue) to highlight nuclei. The right panels show higher magnification images of the VZ (C; arrows denote Ankrd11-positive nuclear foci) or boxed areas (D and E).

(F) Western blot for Ankrd11 in NIH/3T3 cells transfected with control (Con) or one of two *Ankrd11* shRNAs (sh1 or sh2). The blot was reprobed for p130cas.

(G) E12.5 cortical precursors were cultured 3 days and immunostained for Ankrd11 (red) and Ki67, Pax6, or βIII-tubulin (all green). Arrows denote double-positive cells.

(H and I) Precursors were cotransfected with EGFP and control (Con) or *Ankrd11* shRNA (sh1 or sh2) and immunostained for EGFP (green) and Ankrd11 (red) 2 days later (H), and EGFP-positive cells expressing detectable Ankrd11 were quantified by fluorescence intensity (I). (H) shows cells transfected with *Ankrd11* sh2, and the arrow and arrowhead denote EGFP-positive, Ankrd11-negative and EGFP-negative, Ankrd11-positive cells, respectively. $^{**}p < 0.01$, $^{***}p < 0.005$, n = 3 experiments.

(J–P) E12.5 precursors were cotransfected with nuclear EGFP and control (Con) or *Ankrd11* shRNA (sh1 or sh2) and were analyzed 2 or 3 days later. (J and K) Cells were immunostained for EGFP (green, J) and Ki67 (red, J) after 2 days and quantified (K). Arrow denotes a double-positive cell. $^{**}p < 0.01$, n = 4 experiments. (L) EGFP-positive precursors that were BrdU-positive when cultures were exposed to BrdU after 1 day and were analyzed 2 days later. $^{**}p < 0.01$, n = 3 experiments. (M–P) Cultures were immunostained for EGFP (green, M) Pax6 or βIII-tubulin (red, M) at 3 days and quantified (N and P) for double-labeled cells (arrows in M). (O) shows the percentage of EGFP-positive, Pax6-positive cells that were also Ki67-positive, as calculated from (K) and (N). $^{*}p < 0.05$, $^{**}p < 0.01$, n = 3 or 4 experiments.

Scale bars represent 100 μm (C), 20 μm (D and E), and 10 μm (G, H, J, M, and Inset in C). Error bars indicate SEM. See also Figure S1.

RESULTS

Ankrd11 Is Expressed in Precursors and Neurons of the Developing Murine Cortex

To ask about Ankrd11 during neural development, we studied the embryonic cerebral cortex. Quantitative PCR (qPCR) and western blots (Figures 1A and 1B) showed expression of Ankrd11 in the embryonic day 11 (E11) through postnatal day 3 (P3) cortex. Immunostaining showed that Ankrd11 was detectable in nuclear foci of precursors in the E12 ventricular and subventricular (VZ/SVZ) zones (Figure 1C). By E16, Ankrd11 was detectable in nuclei of Pax6-positive radial precursors, the stem cells in this system, and βIII-tubulin positive neurons in the cortical plate (Figures 1D and 1E).

Ankrd11 Regulates Proliferation and Neurogenesis in Cultured Murine Cortical Precursor Cells

To identify a potential function for Ankrd11, we generated two *Ankrd11* small hairpin RNAs (shRNAs) and transfected them into murine NIH/3T3 cells that express endogenous Ankrd11. Western blots showed that both shRNAs were efficacious and validated the specificity of the Ankrd11 antibody (Figure 1F). We used these shRNAs to ask about Ankrd11's function in E12.5 radial precursors that generate neurons in culture (Barnabé-Heider et al., 2005). Ankrd11 immunoreactivity was readily detectable in nuclei of radial precursors expressing Pax6 and Ki67 and in newborn βIII-tubulin-positive neurons (Figure 1G). When cultures were cotransfected with EGFP and *Ankrd11* shRNAs, the shRNAs significantly decreased the percentage of

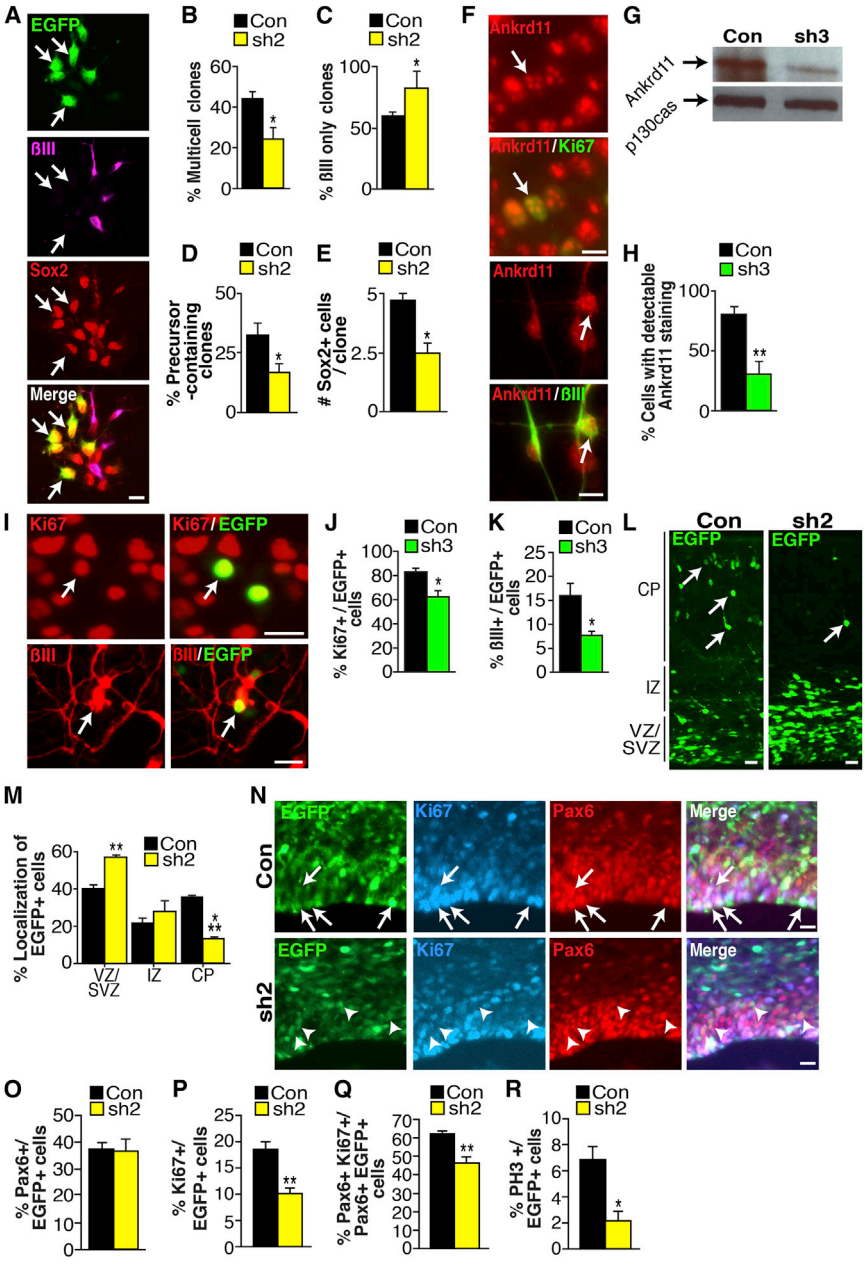

Figure 2. Knockdown of *Ankrd11* in Cultured Murine or Human Cortical Precursors or in the Murine Embryonic Cortex Perturbs Proliferation and Neurogenesis

(A–E) E12.5 precursors were cotransfected with the PB transposase and PB-EGFP reporter, and control (Con) or *Ankrd11* shRNA (sh2), immunostained for EGFP (green, A), Sox2 (red, A), and βIII-tubulin (purple, A) after 3 days, and quantified for clones greater than one cell in size (B), neuron-only clones (C), clones with at least one Sox2-positive precursor (D), and the number of Sox2-positive cells in clones with at least one Sox2-positive precursor (E). Arrows in (A) denote EGFP-positive, Sox2-positive precursors. *p < 0.05, n = 3 experiments.

(F) ESC-derived human cortical precursors immunostained for Ankrd11 (red) and Ki67 or βIII-tubulin (green). Arrows denote double-positive cells.

(G) Western blot of Ankrd11 in HEK293 cells transfected with control (Con) or human *Ankrd11* shRNA (sh3), analyzed after 24 hr. The blot was reprobed for p130cas.

(H–K) Human cortical precursors were co-transfected with EGFP and control (Con) or human-specific *Ankrd11* shRNA (sh3), immunostained 3 days later for EGFP (green, I) and Ankrd11, Ki67 (red, I), or βIII-tubulin (red, I), and quantified for EGFP-positive cells expressing Ankrd11 (H), Ki67 (J), or βIII-tubulin (K). *p < 0.05, **p < 0.01, n = 3 experiments. Arrows in (I) denote double-positive cells.

(L–R) E13/14 cortices were electroporated with EGFP and control (Con) or *Ankrd11* shRNA (sh2), and sections were immunostained 3 days later for EGFP (green, L and N), Pax6 (red, N), and Ki67 (blue, N) or phospho-histone H3, and quantified for the relative location of EGFP-positive cells (M) or the proportions of EGFP-positive, Pax6-positive cells (O), EGFP-positive, Ki67-positive cells (P), EGFP-positive, Pax6-positive cells that also expressed Ki67 (Q), or EGFP-positive, phospho-histone H3-positive cells (R).

In (L) arrows denote cells in the CP, while (N) shows confocal images of the VZ/SVZ, with arrows denoting triple-positive cells and arrowheads denoting EGFP-positive, Pax6-positive, and Ki67-negative cells. *p < 0.05, **p < 0.01, ***p < 0.005, n = 3 embryos each.

Scale bars represent 10 μm (A, F, and I) and 20 μm (L and N). Error bars indicate SEM. See also Figure S2.

transfected cells expressing Ankrd11 (Figures 1H and 1I). *Ankrd11* knockdown did not affect cell survival, as assessed by counting EGFP-positive cells with condensed, apoptotic nuclei ($p > 0.05$) or by immunostaining for cleaved caspase-3 (Figure S1 available online) 2 days posttransfection. Autophagy was also unchanged, as monitored by LC3 immunoreactivity ($p > 0.05$; data not shown).

Ankrd11 knockdown did affect precursor proliferation, as measured by Ki67 immunoreactivity 2 days posttransfection or by adding BrdU to cultures 1 day posttransfection and immunostaining for BrdU 2 days later (Figures 1J–1L). This was not due to a decrease in Pax6-positive radial precursors, but was caused by a decrease in the radial precursor proliferation index (Figures 1M–1O). *Ankrd11* knockdown also reduced transfected βIII-tubulin-positive neurons 3 days posttransfection (Figures 1M and 1P).

Ankrd11 knockdown also decreased radial precursor self-renewal, as shown by clonal analysis with the *piggybac* (PB) transposon, which indelibly marks precursors and their progeny (Gallagher et al., 2013). Specifically, precursors were transfected at low efficiency (Figure S2A) with the PB transposase and PB EGFP reporter, plus control or *Ankrd11* shRNAs, and cultures were immunostained 3 days later for EGFP, the precursor marker Sox2, and βIII-tubulin (Figure 2A). *Ankrd11* knockdown reduced

EGFP-positive multicellular clones and the proportion of clones containing a Sox2-positive precursor, while neuron-only clones were increased (Figures 2B–2D). The number of precursors in clones containing at least one Sox2-positive cell was also reduced (Figure 2E).

Ankrd11 Regulates Proliferation and Differentiation of Human Forebrain Precursors

Since *ANKRD11* mutations are associated with human ASD, we asked whether Ankrd11 was also required for human embryonic stem cell-derived (ESC-derived) cortical precursors, generated as we previously described (Wang et al., 2012). Nuclear Ankrd11 immunoreactivity was detectable in almost all cells in these cultures, including Ki67-positive precursors and βIII-tubulin-positive neurons (Figure 2F). To ask about its function, we generated a human-targeted *Ankrd11* shRNA and confirmed its efficacy by transfecting it into HEK293 cells that express endogenous Ankrd11 (Figure 2G). We cotransfected this shRNA into human neural precursors together with nuclear EGFP. Immunostaining 3 days later showed that the Ankrd11 shRNA significantly reduced Ankrd11 expression in transfected cells (Figures 2H and S2B) and that this knockdown decreased EGFP-positive, Ki67-positive proliferating precursors and EGFP-positive, βIII-tubulin-positive newborn neurons (Figures 2I–2K), as seen in murine precursors.

Ankrd11 Knockdown In Vivo Decreases Radial Precursor Proliferation and Neurogenesis and Causes Mislocalization of Cortical Neurons

To ask whether Ankrd11 regulates cortical development in vivo we in utero electroporated E13/14 cortices with nuclear EGFP and control or *Ankrd11* shRNAs and immunostained sections 3 days later. This approach targets radial precursors in the VZ, many of which differentiate into neurons that migrate through the intermediate zone (IZ) to the cortical plate (CP). *Ankrd11* knockdown altered cell location, with more EGFP-positive cells in the VZ/SVZ and fewer in the CP (Figures 2L and 2M). *Ankrd11* knockdown did not alter EGFP-positive, Pax6-positive radial precursor numbers, but it did reduce Ki67-positive proliferating cells and the radial precursor proliferation index (Figures 2N–2Q and S2C). Mitotic cells expressing phospho-histone H3 were also decreased (Figures 2R and S2D).

We immunostained similar sections for the pan-neuronal marker HuD (Figure 3A). *Ankrd11* knockdown decreased EGFP-positive, HuD-positive neurons by almost 2-fold, and these neurons were misplaced, with fewer in the CP and more in the VZ/SVZ (Figures 3B and 3C). To define the phenotype of these misplaced neurons, we analyzed the layer-specific markers Satb2 and Tbr1 4 days postelectroporation (Figures 3D and 3E). In controls, Satb2-positive and Tbr1-positive cells comprised about 34% and 8% of EGFP-positive cells (Figure 3F), as expected (Tsui et al., 2013). Following *Ankd11* knockdown, Satb2-positive, but not Tbr1-positive, neurons were reduced (Figure 3F). However, Tbr1-positive, but not Satb2-positive, neurons were inappropriately positioned at this time point (Figures 3G and S3).

To ask if these neuronal perturbations persisted, we electroporated E13/14 cortices with the PB transposase and PB EGFP reporter, plus control or *Ankrd11* shRNA, and analyzed sections at P3. In controls, almost all EGFP-positive cells were in layers I to III, but following *Ankrd11* knockdown, they were scattered throughout the cortex, including the SVZ (Figures 3H and 3K). As seen earlier, *Ankrd11* knockdown decreased Satb2-positive, but not Tbr1-positive, neurons, but at this stage both types of cortical neurons were mislocalized to deeper cortical layers and the SVZ (Figures 3I–3N).

Yoda Mice Heterozygous for an *Ankrd11* Missense Mutation in the Repressive HDAC-Binding Domain Also Show Decreased Precursor Proliferation and Mislocalized Neurons

The Yoda mutant mouse was isolated in an *N*-ethyl-*N*-nitrosourea screen for perturbations in bone metabolism (Barbaric et al., 2008) and carries a missense point mutation in the highly conserved C-terminal repression domain of the *Ankrd11* gene (Figure 4A). Homozygous Yoda mice are embryonic lethal, but heterozygous mice (*Ankrd11*$^{Yod/+}$) survive into adulthood with altered bone metabolism and craniofacial abnormalities (Barbaric et al., 2008). Intriguingly, a two amino acid deletion in the analogous region has been found in the human gene (Figure 4A) (Sirmaci et al., 2011). To ask if Yoda mice displayed perturbed neural development, we immunostained E18.5 *Ankrd11*$^{Yod/+}$ cortical sections for Tbr1 and Satb2 (Figures 4B and 4C). Neurons of both phenotypes were misplaced in the VZ/SVZ of *Ankrd11*$^{Yod/+}$ cortices (Figures 4B–4E). In contrast, the morphology of nestin-positive radial precursors, including their basal processes, was apparently similar in *Ankrd11*$^{Yod/+}$ and wild-type cortices (Figures S4A and S4B).

To extend this analysis, we crossed male *Ankrd11*$^{Yod/+}$ mice with wild-type females, injected pregnant mothers with BrdU at gestational day 13.5, and immunostained sections 5 days later. BrdU-positive cells were mislocalized in Yoda cortices (Figure 4G). We quantified this, using similarly aged wild-type and Yoda sections triple labeled for Satb2, Pax6, and the intermediate progenitor marker Tbr2 to define the cortical regions (Figures 4F and S4C). This analysis showed significantly more BrdU-positive cells in the *Ankrd11*$^{Yod/+}$ IZ and fewer in the CP (Figure 4H). Double labeling also showed significantly fewer BrdU-positive, Ki67-positive precursors in the VZ/SVZ (Figures 4I and 4K) and fewer total BrdU-positive, Satb2-positive cells (Figures 4J, 4L, and S4D) in *Ankrd11*$^{Yod/+}$ cortices. These changes were not due to cell senescence, as monitored by SA-β-gal staining (data not shown). Thus, as seen with acute *Ankrd11* knockdowns, a heterozygous Yoda mutation caused decreased precursor proliferation, and perturbed genesis and localization of neurons.

Ankrd11$^{Yod/+}$ Mice Have Perturbations in Adult Neural Precursors and Are Behaviorally Abnormal

We asked whether adult neural precursor cells (NPCs) from *Ankrd11*$^{Yod/+}$ mice were also perturbed, initially focusing on the adult SVZ. We injected adult wild-type and *Ankrd11*$^{Yod/+}$ mice with BrdU and immunostained SVZ sections 24 hr later. *Ankrd11*$^{Yod/+}$ mice had significantly fewer BrdU-positive SVZ cells and fewer Sox2-positive NPCs that were BrdU-positive (Figures 5A–5C). We also asked about adult-born olfactory bulb neurons by immunostaining olfactory bulb sections 1 month following multiple BrdU injections. Adult-born BrdU-positive, NeuN-positive olfactory bulb neurons were significantly reduced in *Ankrd11*$^{Yod/+}$ mice (Figures 5D and 5E).

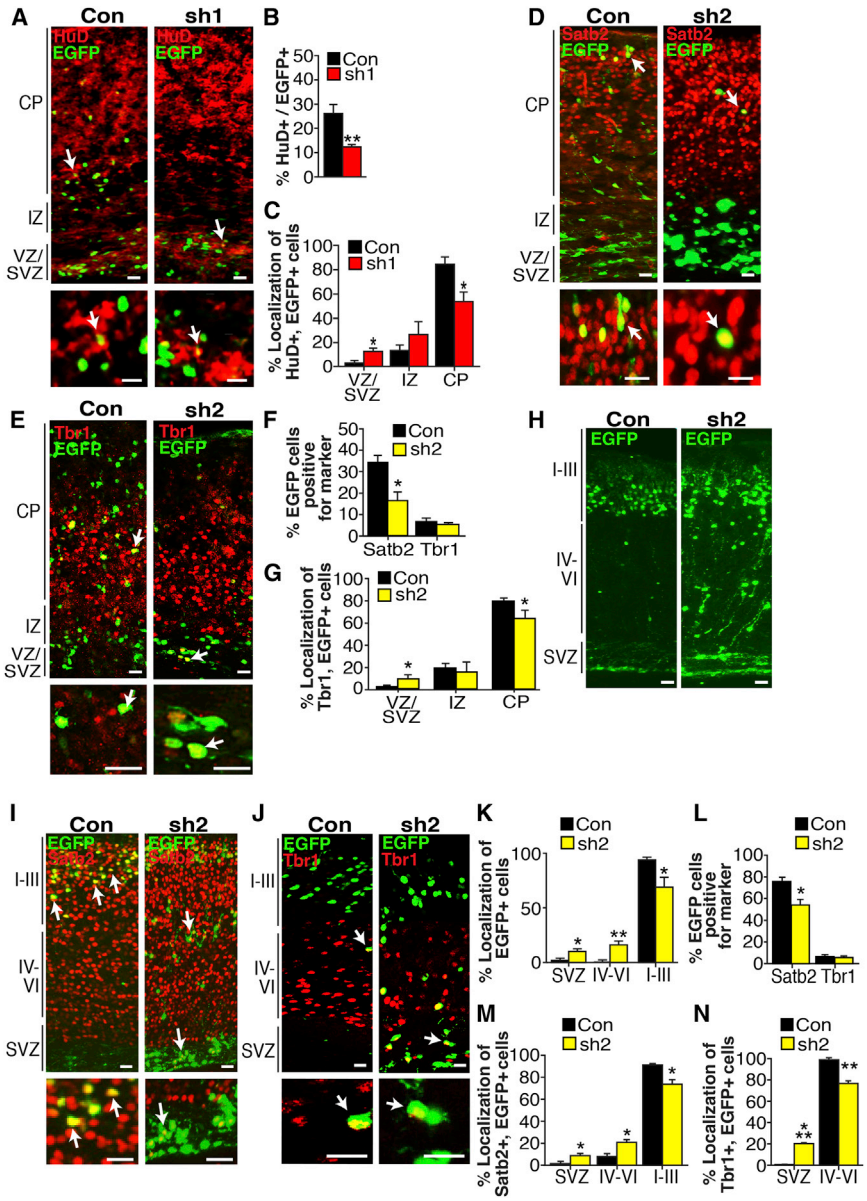

Figure 3. *Ankrd11* Knockdown in Cortical Precursors Perturbs the Numbers and Positions of Developing Neurons

(A–G) E13/14 cortices were electroporated with EGFP and control (Con) or *Ankrd11* shRNA (sh1 or sh2), and sections were immunostained 3 (A–C) or 4 (D–G) days later for EGFP (green) and HuD (red, A), Satb2 (red, D), or Tbr1 (red, E) and quantified for the proportions of EGFP-positive cells expressing HuD (B) or Satb2 and Tbr1 (F) or the relative location of EGFP-positive, marker-positive cells (C and G). In (A), (D), and (E), higher magnification images of double-labeled cells (arrows) are shown at the bottom. *$p < 0.05$, **$p < 0.01$, $n = 3$ embryos each.

(H–N) E13/14 cortices were electroporated with PB transposase and PB EGFP reporter and control (Con) or *Ankrd11* (sh2) shRNA, and sections were immunostained at P3 for EGFP (green) and Satb2 (red, I) or Tbr1 (red, J) and quantified for the relative location of EGFP-positive, marker-positive cells in the different cortical layers (K, M, and N) or the proportions of EGFP-positive cells expressing Satb2 or Tbr1 (L). In (I) and (J), higher magnification images of double-labeled cells (arrows) are shown at the bottom. *$p < 0.05$, **$p < 0.01$, ***$p < 0.005$, $n = 3$ each.

Scale bars represent 10 μm (D, lower right panel and E, lower right panel) and 20 μm (A, D, E, and H–J). Error bars indicate SEM. See also Figure S3.

We also examined the other adult NPC niche, the subgranular zone (SGZ) of the dentate gyrus, by analyzing hippocampal sections 24 hr following BrdU injection. The *Ankrd11*$^{Yod/+}$ SGZ contained fewer BrdU-positive cells, Sox2-positive cells, and double-labeled BrdU-positive, Sox2-positive proliferating NPCs (Figures 5F–5H and S5A). Doublecortin-positive neuroblasts and newborn neurons were also reduced in the *Ankrd11*$^{Yod/+}$ SGZ (Figures 5I and S5B). We also asked about mature adult-born neurons, administering BrdU and immunostaining hippocampal sections 1 month later (Figure S5C). BrdU-positive, NeuN-positive adult-born neurons in the dentate gyrus were significantly decreased in *Ankrd11*$^{Yod/+}$ mice (Figure 5J). Thus, Ankrd11 is also important for adult NPC proliferation and neurogenesis.

Since *ANKRD11* mutations are associated with intellectual disability and ASD in humans, we characterized the Yoda mice behaviorally. Initially, we used the open field test to ask about general levels of activity. *Ankrd11*$^{Yod/+}$ mice traveled significantly less distance in the open field than their wild-type counterparts (Figure 5K). This decrease was due to a reduction in total time spent traveling (400.73 ± 25.2 s for *Ankrd11*$^{Yod/+}$ versus 478.9 ± 22.8 for wild-types, $p = 0.03$) rather than a change in movement velocity, which was similar for both groups (33.7 ± 1.15 cm/s for *Ankrd11*$^{Yod/+}$ and 35.8 ± 1.12 cm/s for wild-types; $p > 0.05$).

We then tested the *Ankrd11*$^{Yod/+}$ mice in a three-chamber social preference test (Moy et al., 2004) that assays social interactions with an unfamiliar mouse, a behavior that is perturbed in some mouse models of ASD (Crawley et al., 2007; Molina et al., 2008; Carter et al., 2011). To perform this test, mice were placed in and allowed to habituate to a three-chamber environment; wild-type and *Ankrd11*$^{Yod/+}$ mice spent equivalent percentages of time in each of the compartments during this habituation ($p > 0.05$). We then put an unfamiliar mouse (stranger 1 [Str1]) in one of the chambers. As predicted, wild-type mice spent more time in the chamber side containing the unfamiliar mouse relative to that containing an inanimate target (Emt) (Figure 5L). In contrast, *Ankrd11*$^{Yod/+}$ mice showed no significant preference (Figure 5L). Similar results were obtained whether the unfamiliar mouse was placed in chamber 1 or chamber 3 ($p > 0.05$).

We then asked whether the mice would prefer a new unfamiliar mouse over the now-familiar stranger 1 mouse by replacing the

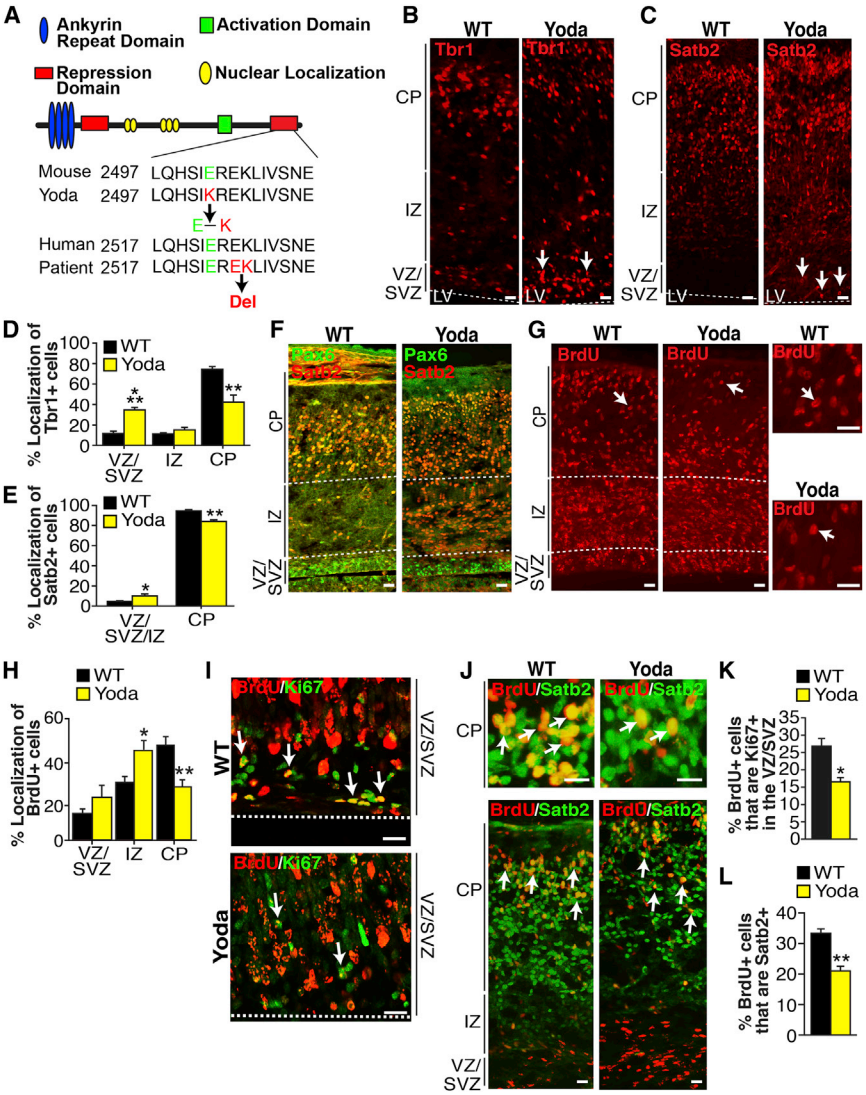

Figure 4. *Ankrd11*$^{Yod/+}$ Embryos Display Deficits in Cortical Precursor Proliferation, Neuronal Numbers, and Neuronal Localization

(A) Schematic of Ankrd11 showing the Yoda missense mutation (Barbaric et al., 2008), and a human deletion in the same region (Sirmaci et al., 2011).

(B–E) E18.5 *Ankrd11*$^{Yod/+}$ (Yoda) and wild-type (WT) cortical sections were immunostained for Tbr1 (B) or Satb2 (C), and the relative location of Tbr1-positive (D) and Satb2-positive (E) neurons were quantified. Arrows in (B) and (C) denote misplaced neurons in the VZ/SVZ. *$p < 0.05$, **$p < 0.01$, ***$p < 0.001$, $n = 4$ each.

(F–L) E18.5 cortical sections from *Ankrd11*$^{Yod/+}$ (Yoda) and wild-type (WT) embryos BrdU-labeled at E13.5 were immunostained for BrdU (red, G, I, and J) and Ki67 (green, I) or Satb2 (green, J), and quantified for relative location of BrdU-positive cells (H), BrdU-positive, Ki67-positive cells in the VZ/SVZ (K), or total BrdU-positive, Satb2-positive cells (L). To define the cortical regions in (G) and (H), E18.5 sections were immunostained for Pax6 (green, F), Satb2 (red, F), and Tbr2 (see Figure S4C). The IZ/CP border for quantification was defined by the apical-most edge of the Satb2-positive neurons in the wild-type sections, as shown by hatched lines. (I) shows only the VZ/SVZ and dotted lines indicate the apical edge. Arrows denote single (G) or double-labeled (I and J) cells. *$p < 0.05$, **$p < 0.01$, $n = 4$ each.

Scale bars represent 20 μm. Error bars indicate SEM. See also Figure S4.

inanimate object with a second stranger mouse (stranger 2 [Str2]). Wild-type mice spent significantly more time in the chamber containing stranger 2 than in that containing stranger 1. In contrast, the *Ankrd11*$^{Yod/+}$ mice did not prefer the stranger 2 mouse (Figures 5M and 5N).

We then assayed repetitive behaviors, which are thought to be ASD-like, by measuring self-grooming (Carter et al., 2011). Mice were placed into a cage for 1 hr to habituate and were then observed for 10 min. Over this period, *Ankrd11*$^{Yod/+}$ mice spent twice as much time grooming themselves as did their wild-type littermates (Figure 5O). Thus, *Ankrd11*$^{Yod/+}$ mice display behaviors that could reflect cognitive dysfunction and ASD-like perturbations.

Perturbations in Ankrd11 Cause Global Changes in Gene Expression in Cortical Precursors

To ask if Ankrd11 is a transcriptional coregulator, we compared gene expression in neural precursors from embryonic Yoda versus wild-type mice. To do so, we expanded E14 cortical precursors as neurospheres for 6 days in EGF and FGF2 and then passaged and expanded these as secondary neurospheres for analysis. Simultaneously, we grew the same cells at clonal density for quantification. The clonal analysis showed that the *Ankrd11*$^{Yod/+}$ embryonic cortex contained only about half as many neurosphere-initiating cells (Figure 6A). Moreover, these were decreased in their ability to self-renew, since fewer secondary spheres were generated when they were passaged at clonal density (Figure 6B), confirming that Ankrd11 is required for cortical precursor self-renewal.

We analyzed the transcriptome of the expanded secondary neurospheres by microarray, comparing six and five biological replicates of *Ankrd11*$^{Yod/+}$ and wild-type neurospheres, respectively, with the Affymetrix GeneChip Mouse Gene 2.0 Array (Gene Expression Omnibus (GEO) database accession number GSE63303). Spearman rank correlation (Figure 6C) showed that these two populations differed at the transcriptome level. In addition, while the wild-type neurosphere samples were all relatively similar to each other, the *Ankrd11*$^{Yod/+}$ neurospheres showed more heterogeneity, potentially due to variable penetrance of the heterozygote phenotype (Figure 6C).

To further investigate these differences, we performed differential expression analysis to compare the wild-type and *Ankrd11*$^{Yod/+}$ data sets using the Parteks Genomic Suite; 761

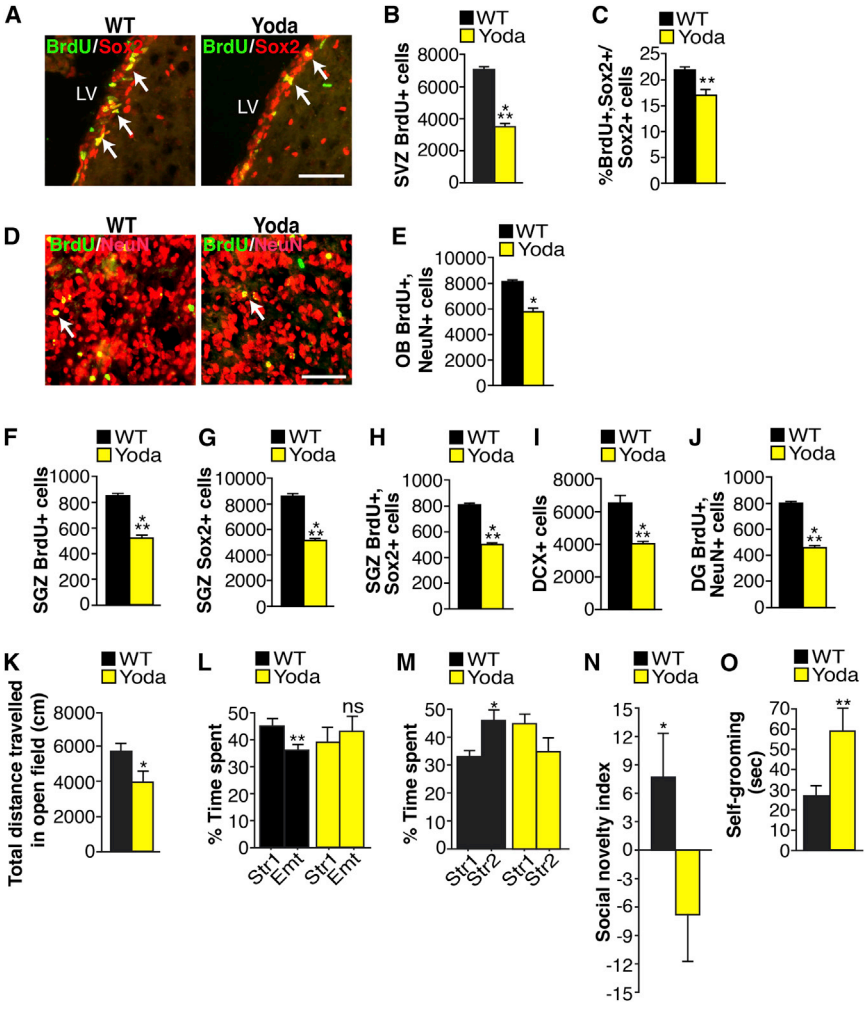

Figure 5. Perturbations in Neural Precursors, Adult-Born Neurons, and Behavior in Adult *Ankrd11*$^{Yod/+}$ Mice

(A–J) Adult 6-month-old *Ankrd11*$^{Yod/+}$ (Yoda) mice and their wild-type littermates (WT) were injected with BrdU, and the SVZ, olfactory bulb (OB), or dentate gyrus (DG) were analyzed 24 hr (A–C and F–I) or 30 days (D, E, and J) later. (A–C) Sections spanning the SVZ 24 hr postinjection were immunostained for BrdU (green, A) and Sox2 (red, A), and the total BrdU-positive cells (B) and percentage of Sox2-positive cells that were BrdU-positive (C) were quantified. Arrows denote double-labeled cells. **$p < 0.01$, ***$p < 0.001$, n = 3 animals each. (D and E) Sequential olfactory bulb sections 30 days postinjection were immunostained for BrdU (green, D) and NeuN (red, D), and the total BrdU-labeled, NeuN-positive neurons were quantified (E). Arrows show double-labeled neurons. *$p < 0.05$, n = 3 each. (F–I) Quantification of sections 24 hr post-BrdU injection for total subgranular zone (SGZ) cells that were BrdU-positive (F), Sox2-positive (G), BrdU- and Sox2-positive (H) or doublecortin-positive (I). ***$p < 0.001$, n = 3 each. (J) Quantification 30 days postinjection for total BrdU-positive, NeuN-positive dentate gyrus neurons. ***$p < 0.001$, n = 3 each.

(K–O) Adult *Ankrd11*$^{Yod/+}$ (Yoda) and wild-type (WT) littermates were analyzed behaviorally. (K) Total distance traveled (centimeters) in the open field test. *$p < 0.05$, n = 15 WT and 9 *Ankrd11*$^{Yod/+}$ mice. (L and M) Percentage of time spent in the stranger 1 (Str1) chamber versus the empty container (Emt) chamber (L) and in the stranger 1 (Str1) chamber versus the new stranger 2 (Str2) chamber (M) during the three-chamber sociability test. *$p < 0.05$, **$p < 0.01$, two-way repeated-measures ANOVA (genotype X side) with Bonferroni's post hoc analysis, n = 15 WT and 9 *Ankrd11*$^{Yod/+}$ mice, ns = not significant. (N) Social novelty index, calculated as [$time_{Str2}/(time_{Str2} + time_{Str1})$] × 100 − 50 (Jamain et al., 2008). *$p < 0.05$, n = 15 WT and 9 *Ankrd11*$^{Yod/+}$ mice. (O) Total time spent self-grooming (seconds) over a 10 min test period. **$p < 0.01$, n = 15 WT and 7 *Ankrd11*$^{Yod/+}$ mice.

Scale bars represent 100 μm (A and D). Error bars indicate SEM. See also Figure S5.

genes, or approximately 3% of those analyzed, were significantly differentially expressed (using false discovery [FDR] p value < 0.1 and fold change [FC] > 1.1 or < −1.1) (Figure 6D and Table S1). These genes clearly distinguished the *Ankrd11*$^{Yod/+}$ and wild-type precursors, as shown in a heatmap (Figure 6E). We validated these results by real-time qPCR, confirming mRNAs that were upregulated (*Notch1*, *Slc1A2*, *Mll5*, *Fzd3*, *Sox6*, *Ncor1*, *Foxn3*, *Med13*, and *Ncoa1*) or downregulated (*Eya2*, *Med10*, *Foxp1*, and *Gabrg1*) in *Ankrd11*$^{Yod/+}$ neurospheres. This analysis validated the microarray data (Figure 6F), showing a Pearson correlation coefficient of 0.995 (Figure 6G).

We then subjected the 761 differentially expressed genes to gene ontology and pathway analysis. This analysis showed that the enriched pathways were diverse in terms of their functions (Figure 6H and Table S2). Intriguingly, two disorder categories with the highest p values were schizophrenia and abnormal morphology of the nervous system (Figure 6H), consistent with the phenotypes that we observed in the Yoda mice.

Ankrd11 Associates with Chromatin, and Histone Acetylation Is Increased, in *Ankrd11*$^{Yod/+}$ Neural Precursors

Since Ankrd11 can bind HDACs, we asked whether chromatin acetylation was altered in Yoda mice, initially isolating total histones from adult *Ankrd11*$^{Yod/+}$ and wild-type cortices. Western blots demonstrated increased acetylation of histones H3 and H4 at H3K9, H4K5, H4K8, and H4K16 (Figure 7A), all known HDAC3 target sites (Rudenko and Tsai, 2014). We then examined histone acetylation in the E14 cortical neurospheres used for the microarrays. Western blots showed that, relative to total histone H4, acetylation in the *Ankrd11*$^{Yod/+}$ neurosphere chromatin was increased at H4K5, H4K8, H4K16, and H3K9, but unaltered at H3K14 and H3K27 (Figures 7B and 7C).

To ask if altered histone acetylation could explain the observed gene expression changes, we analyzed H4K16 acetylation on genes upregulated in *Ankrd11*$^{Yod/+}$ neurospheres, focusing on *Notch1*, *Slc1A2*, *Mll5*, *Fzd3*, *Sox6*, and *Ncor1*. To do so, we immunoprecipitated cortical neurosphere chromatin

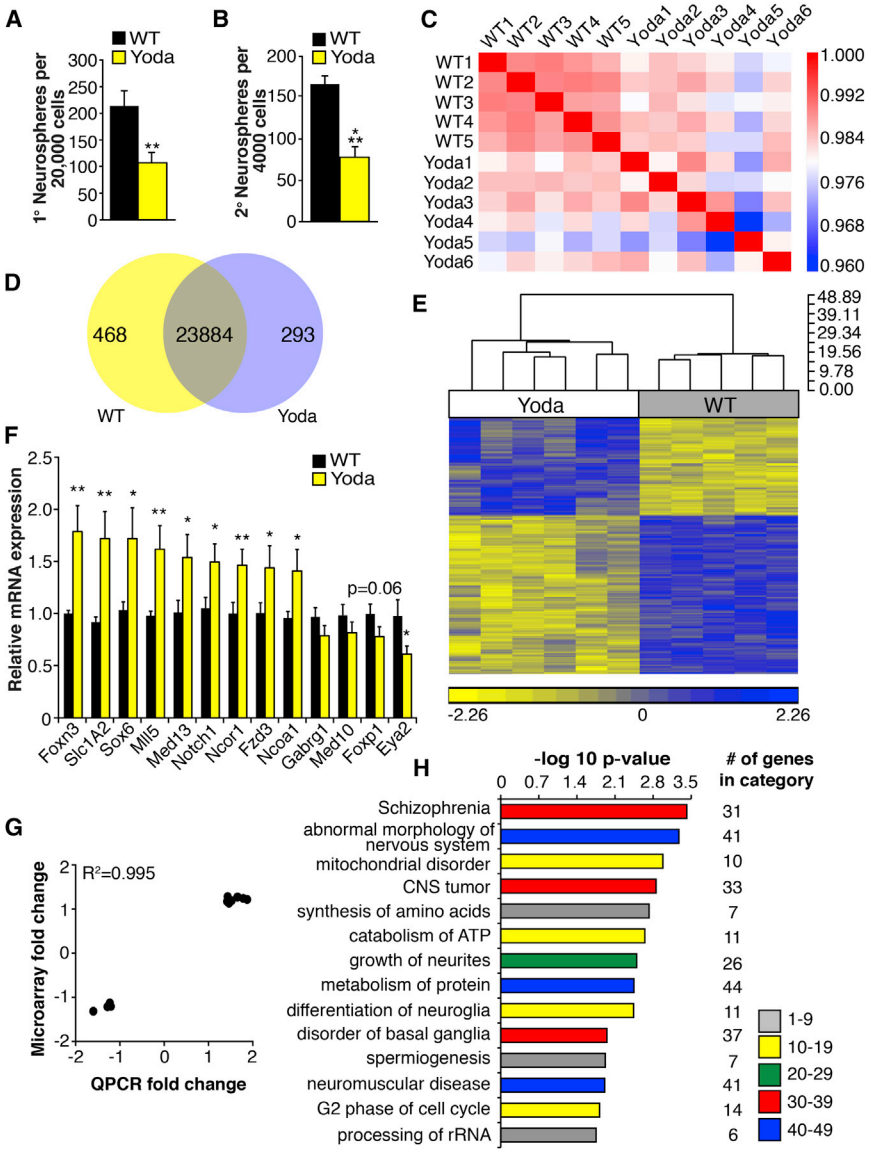

Figure 6. Alterations in Self-Renewal and Gene Expression in Embryonic Cortical Precursors from *Ankrd11*$^{Yod/+}$ Mice

Analysis of *Ankrd11*$^{Yod/+}$ (Yoda) and wild-type (WT) E14 cortical neurospheres.

(A and B) Number of primary (A) and secondary (B) neurospheres generated from E14 cortical cells at clonal density $^{**}p < 0.01$, $^{***}p < 0.005$, n = 6 WT and 7 *Ankrd11*$^{Yod/+}$ embryos.

(C–E) Microarray analysis of six and five independent isolates of *Ankrd11*$^{Yod/+}$ and wild-type secondary cortical neurospheres (Yoda1-6 and WT1-5). (C) Spearman rank correlation matrix computed for the microarray experiments based upon all 41,345 probe sets, with red and blue representing the most and least highly correlated samples, respectively. (D) Venn diagram of a pair-wise comparison showing genes that were significantly different (using FDR p value < 0.1 and FC > 1.1 or < −1.1). (E) A heatmap of the 761 genes that were significantly differentially expressed in (D), clustered using Partek Genomics Suite. The genes are shown in Table S1.

(F) qRT-PCR analysis of genes selected from the microarray analysis. $^{*}p < 0.05$, $^{**}p < 0.01$, n = mRNA from six secondary neurosphere samples each.

(G) Correlation of fold change in gene expression (*Ankrd11*$^{Yod/+}$ versus WT neurospheres) for the microarrays versus the qRT-PCRs. Each point represents the average value of genes in (F) from at least 6 mRNA preparations each. Pearson's correlation coefficient $R^2 = 0.995$, p = 0.00003.

(H) Significantly differentially expressed genes from (E) were analyzed using Ingenuity pathway analysis, and the top pathways are presented. Categories are color-coded based on the number of genes they contain. Genes in each category are shown in Table S2. See also Tables S1 and S2.

with anti-H4K16ac or anti-H4 and analyzed genomic elements located within 1 kb of the 5′ untranslated region by qPCR, focusing on sequences associated with acetylated H3K27 in E14.5 whole brain (ENCODE database, GEO accession number GSM1000094) (Rosenbloom et al., 2013). This analysis showed that, in *Ankrd11*$^{Yod/+}$ neurospheres, H4K16 acetylation was significantly increased on the *Notch1*, *Slc1A2*, *Mll5*, *Fzd3*, and *Sox6* genomic elements (Figure 7D).

To ask if these genomic loci were direct targets of Ankrd11, we performed chromatin immunoprecipitation (ChIP) with anti-Ankrd11. Since the *p21* gene is directly regulated by Ankrd11 (Neilsen et al., 2008), we initially validated the Ankrd11 antibody for ChIP with the *p21* promoter (Neilsen et al., 2008). This analysis showed that anti-Ankrd11 immunoprecipitates were significantly enriched for the *p21* gene element relative to nonspecific IgG and to the desert region on chromosome 15, which is at least 500 kbp away from any known gene (Figure S6A). We then performed ChIP for the selected genes in wild-type neurospheres. Ankrd11 was significantly associated with *Notch1*, *Slc1A2*, *Mll5*, *Fzd3*, *Sox6*, and *Ncor1* gene elements, but not with *Foxn3*, *Med10*, or *Ncoa1* gene elements (Figure 7E). Importantly, none of these latter gene elements showed significantly altered H4K16 acetylation in *Ankrd11*$^{Yod/+}$ neurospheres (p > 0.06; data not shown).

Ankrd11 Controls Neural Precursor Proliferation via HDAC3 and Histone Acetylation

The strong correspondence between Ankrd11 chromatin association sites and increased H4K16 acetylation at those sites in *Ankrd11*$^{Yod/+}$ neurospheres suggests that Ankrd11 directly regulates HDAC function. To test this idea, we focused on HDAC3, which interacts with Ankrd11 when overexpressed (Zhang et al., 2004). Immunostaining of cultured precursors showed that HDAC3 was present in some Ankrd11-positive nuclear foci (Figure 7F). To ask if they directly associated, we performed proximity ligation assays, which provide a positive readout when antibody targets are within 40 nm of each other (Söderberg et al., 2006). Bright fluorescent nuclear puncta were observed when anti-Ankrd11 and anti-HDAC3 were

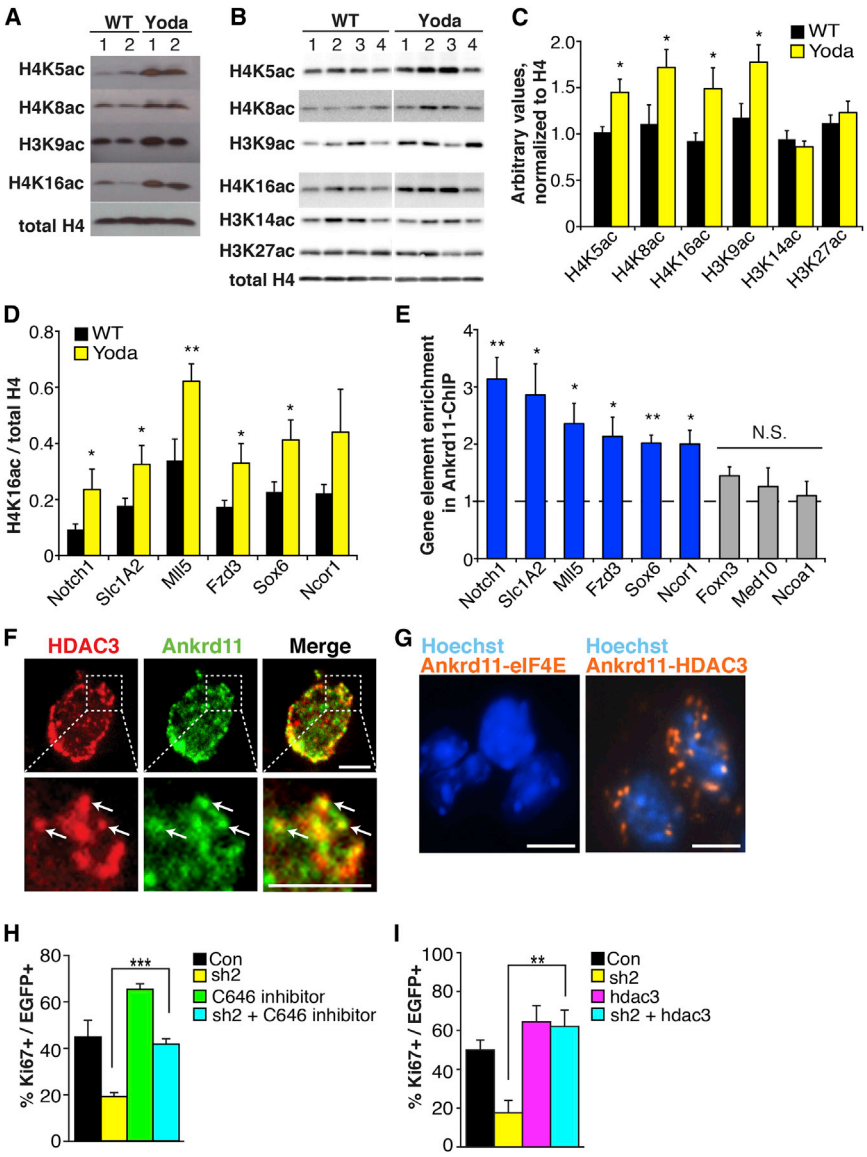

Figure 7. Ankrd11 Associates with Chromatin, Histone Acetylation Is Increased in *Ankrd11*$^{Yod/+}$ Neural Precursors, and This Causes Decreased Precursor Proliferation

(A–C) Western blots with acetylation-site specific histone antibodies (H4K5ac, H4K8ac, H3K9ac, H4K16ac, H3K14ac, H3K27ac) in total histones isolated from adult *Ankrd11*$^{Yod/+}$ (Yoda) and wild-type (WT) cortices (A) or in chromatin protein from E14 cortical secondary neurospheres (B). Samples were also probed for total histone H4, and (C) shows chemiluminescence quantification relative to H4 of blots as in (B). *$p < 0.05$, $n = 7$ neurosphere samples each.

(D) ChIP-qPCR of E14 cortical neurosphere chromatin immunoprecipitated with anti-H4K16ac or anti-H4. Genomic loci associated with anti-H4K16ac or anti-H4 were expressed as percent input, and H4K16ac values were normalized to total H4 values. *$p < 0.05$, **$p < 0.01$, $n = 5$ neurosphere samples each.

(E) ChIP-qPCR of wild-type E14 neurosphere chromatin immunoprecipitated with anti-Ankrd11 or nonspecific IgG (dashed line). Genomic loci associated with anti-Ankrd11 or IgG were expressed as percent input and normalized to IgG (equated to 1). Blue and gray bars designate loci that were significantly (*$p < 0.05$, **$p < 0.01$) or not significantly associated (N.S.) with Ankrd11, respectively. $n = 4$ E14 cortical neurosphere samples.

(F) Confocal images of E12.5 cultured cortical precursor nuclei immunostained for Ankrd11 (green) and HDAC3 (red). The boxed areas are also shown at higher magnification on the bottom. Arrows denote colocalization.

(G) Cortical precursor nuclei (blue, Hoechst) following the proximity ligation assay with anti-HDAC3 and anti-Ankrd11 (right, red puncta) or, as a negative control, anti-eIF4E and anti-Ankrd11 (left).

(H and I) E12.5 precursors were cotransfected with EGFP and control (Con) or *Ankrd11* (sh2) shRNA. Cells were treated with 500 nM C646 HAT inhibitor after 2 days (H), or they were cotransfected with a control or *HDAC3* expression vector (I). Three days posttransfection, cells were immunostained for EGFP and Ki67 and quantified. **$p < 0.01$, ***$p < 0.001$, analyzed by ANOVA with Fisher's post hoc test. $n = 3$ experiments each.

Scale bars represent 5 μm (F) and 10 μm (G). Error bars indicate SEM. See also Figure S6.

combined, but not when anti-eIF4E, which robustly immunostains cortical precursors (Yang et al., 2014), was combined with either anti-Ankrd11 or anti-HDAC3 (Figures 7G and S6B).

These data identify an Ankrd11/HDAC3 complex in cortical precursors and suggest that *Ankrd11* mutation or knockdown disrupts this complex and thus abnormally elevates histone acetylation. We therefore asked whether rebalancing histone acetylation with the HAT inhibitor C646 (Bowers et al., 2010) would rescue the *Ankrd11* knockdown-induced changes, focusing on precursor proliferation. Cultured precursors were transfected with EGFP and control or *Ankrd11* shRNA, were treated with 500 nM C646 after 1 day, and were stained for Ki67 2 days later. C646 completely rescued the reduced proliferation seen following *Ankrd11* knockdown (Figure 7H).

Finally, we asked whether ectopic HDAC3 expression could also rescue this proliferation phenotype. Cultured precursors were cotransfected with EGFP and *Ankrd11* shRNA with or without an *HDAC3* expression plasmid. Immunostaining 3 days later demonstrated that HDAC3 had no effect on Ki67-positive cells under basal conditions but completely rescued the decreased proliferation caused by *Ankrd11* knockdown (Figure 7I).

DISCUSSION

ASD is a constellation of behaviorally related neurodevelopmental disorders with a strong genetic component. Many genes have been associated with ASD, and one key question is how they

cause ASD-type behaviors. In this regard, a subset of these genes regulates synaptogenesis, but a further subset has no identified function in the brain. Here, we have focused upon one of the latter genes encoding a nuclear protein, Ankrd11, which has been implicated as a transcriptional coregulator. Individuals with *ANKRD11* mutations display neurodevelopmental phenotypes, including aspects of ASD, cognitive disability (Sirmaci et al., 2011; Lo-Castro et al., 2013; Iossifov et al., 2014), and neuroanatomical perturbations such as periventricular heterotopias (Willemsen et al., 2010) Here, we show that Ankrd11 plays an important role during neural development, acting to determine appropriate histone acetylation and gene expression and thus proliferation of embryonic neural precursors and the genesis and positioning of newborn neurons. Moreover, we show that disruption of Ankrd11 causes long-lasting changes in the adult forebrain together with ASD-like behaviors, thereby providing an explanation for the perturbations that occur when *ANKRD11* is mutated in humans.

How does Ankrd11 regulate neural development? We propose it functions as a transcriptional coregulator that binds to HDAC3 and potentially other HDACs, and in so doing regulates histone acetylation, gene expression, and ultimately the biology of developing precursors and neurons. This model is based upon previous work in cell lines together with data here showing that (1) HDAC3 and Ankrd11 colocalized and associated in cortical precursors, (2) histone acetylation was increased and gene expression broadly perturbed in Yoda cortical precursors, (3) for some genes, this increased histone acetylation and gene expression correlated with Ankrd11 chromatin association, and (4) rebalancing histone acetylation by overexpression of HDAC3 or pharmacological HAT inhibition rescued the *Ankrd11* knockdown-mediated decrease in precursor proliferation. This model is consistent with previous studies showing that disruption of HDAC3 altered neural precursor proliferation and neuronal differentiation (Sun et al., 2007; Castelo-Branco et al., 2014) and caused increased H4K8 acetylation coincident with changes in neuronal gene expression (McQuown et al., 2011), phenotypes that are reminiscent of those seen following disruption of Ankrd11.

A number of additional intriguing conclusions came from the Yoda cortical precursor gene expression analyses. First, the type of genes that were deregulated in Yoda precursors was diverse, suggesting that Ankrd11 likely plays a relatively global role as a transcriptional coregulator. Many of these deregulated genes encode known regulators of cortical development, including transcriptional or chromatin regulators such as *SOX6*, *RelA*, *RB1*, *Notch1*, *NCOA1*, *NCOR1*, *NCOR2*, *MLL5*, *ARID2*, *MED10*, *MED13*, *WDR61*, *WDR26*, *FOXP1*, *ZEB2*, *ATF5*, *EYA2*, and *FOXN3* and signaling molecules such as *PTCH1*, *DCC*, *SEMA5B*, *FZD3*, and, *SPRY1* (see Table S1). Our ChIP studies indicate that at least a subset of these genes are directly associated with Ankrd11. Thus, Ankrd11 may coordinately regulate multiple genes important for neural development by modulating or fine-tuning their expression. Second, one robust disease association for the deregulated genes was schizophrenia. Since many genes implicated in ASD are also associated with schizophrenia (Mullin et al., 2013; McCarthy et al., 2014), then our finding that mutation of an ASD-associated gene caused changes in genes implicated in schizophrenia supports the idea of a common cellular network.

Our data show that Yoda mice, like humans carrying one mutant *ANKRD11* allele, exhibit neuroanatomical perturbations such as neurons misplaced around the lateral ventricles (periventicular heterotopias) and ASD-like behaviors. These findings are intriguing in light of the recent description of patches of cortical disorganization in children with autism (Stoner et al., 2014) and support the idea that the Yoda mouse is a model for the human situation. However, these findings also raise the possibility that there are multiple mechanisms that can lead to ASD-like behavior, both in mice and humans. While one likely mechanism involves later aspects of circuit formation like synaptogenesis, our findings suggest a second important mechanism involving early changes in neurogenesis and neuronal specification and/or localization that ultimately provide an aberrant template upon which to build the circuitry that is essential for normal cognitive function.

EXPERIMENTAL PROCEDURES

Animals and Genotyping

All animal use was approved by the Hospital for Sick Children Animal Care Committee in accordance with Canadian Council of Animal Care policies. *Ankrd11*$^{Yod/+}$ mice (Barbaric et al., 2008) were from the European Mouse Mutant Archive and genotyped as in Supplemental Experimental Procedures. CD1 mice (Charles River) were used in all other experiments.

Plasmids and shRNAs

We used previously published plasmids, pEF-EGFP, PCAG-PB-EGFP, and PCAG-Pbase (Gallagher et al., 2013). The *HDAC3* plasmid (Origene) was in the pCMV6 backbone and *Ankrd11* shRNAs (EZ Biolabs) were in the pGCsi backbone. shRNA sequences are in Supplemental Experimental Procedures.

Cell Cultures

E12.5 cortical precursors were cultured and transfected at 125,000–150,000 cells/ml as described (Barnabé-Heider et al., 2005). E14 cortical neurospheres were cultured and passaged at 6 days under standard conditions at 50 cells/μl for biochemistry and clonal density (Coles-Takabe et al., 2008) for quantification, counting spheres with at least 10 cells. For human precursors, Hes2 ESCs were differentiated as described (Wang et al., 2012). HEK293 cells and NIH/3T3 cells were cultured as described (Zander et al., 2014). Additional details are in Supplemental Experimental Procedures.

In Utero Electroporations and BrdU Experiments

In utero electroporations and embryonic BrdU experiments were performed as described (Zander et al., 2014). For adult BrdU studies, 6-month-old mice were injected once with 100 mg/Kg BrdU or five times with 60 mg/kg BrdU and analyzed 24 hr or 30 days later, respectively, by counting 10 SVZ, dentate gyrus or olfactory bulb sections, sampled every tenth section, as described (Cancino et al., 2013) and detailed in Supplemental Experimental Procedures.

Immunocytochemistry, Proximity Ligation Assays, Microscopy, and Quantification

Immunocytochemistry of cultured cells and cryopreserved or paraffin-embedded tissue was performed as described (Cancino et al., 2013; Zander et al., 2014). Proximity ligation assays were carried out using Duolink in situ red starter kit for mouse/rabbit as per manufacturer's instructions (Olink Bioscience). For culture knockdowns or for clonal analysis, over 100 transfected cells or clones per condition per experiment were quantified. For Ankrd11 expression levels, Northern Eclipse (Empix) software was used to determine signal over a threshold level. For in vivo analysis, coronal sections were analyzed using a Zeiss Pascal confocal microscope. Four sections per embryo were analyzed, taking three pictures covering the VZ, SVZ, IZ, and CP of sections at equivalent anatomic levels.

qRT-PCR and Microarrays

RNA and cDNA preparation, primers and qRT-PCR methods are in Supplemental Experimental Procedures. For microarrays, 5.5 μg of cDNA was hybridized to the Affymetrix Gene Chip Mouse Gene 2.0 ST and results analyzed using Partek Genomics Suite 6.6. Only probesets for annotated genes were used for differential expression analysis. ANOVA statistics were calculated and the genes with FDR p value < 0.1 and FC > 1.1 or < −1.1 were considered statistically significant. Affymetrix Expression Console 1.1 was used for Spearman rank correlations, Partek Genomics Suite 6.6 for unbiased hierarchical clustering and heatmaps, and Ingenuity Pathway Analysis (IPA, version 18488943) for gene ontology pathways. Microarray data can be found at GEO accession number GSE63303.

Chromatin Preparations and Immunoprecipitation Analysis

Chromatin from secondary passage neurospheres was prepared as described (Savage et al., 2009; Supplemental Experimental Procedures). ChIP was performed as described (Savage et al., 2009) with 20 μg chromatin and 4 μg anti-Ankrd11 (Neilsen et al., 2008) or nonspecific rabbit IgG (Millipore), or 2 μg chromatin and 2 μg anti-H4 or anti-H4K16ac (Millipore). Chromatin was reverse crosslinked, DNA purified, and Ankrd11-, H4K16ac-, and total H4-bound chromatin calculated as percent input by qPCR with primers listed in Supplemental Experimental Procedures. To be considered a true association, enrichment with a specific antibody was compared to nonspecific IgG ($p < 0.05$). All primers were validated and qPCR assays were performed in accordance with Minimum Information for Publication of Quantitative Real-Time PCR Experiments guidelines.

Western Blots and Densitometry

Westerns for proteins other than histones were performed as described (Barnabé-Heider et al., 2005). For cortical histones, tissue was dissected in PBS plus 5 mM sodium butyrate to retain acetylation, and histones were extracted and analyzed as described in Supplemental Experimental Procedures. For neurospheres, 1 μg chromatin was reverse-crosslinked at 65°C for 16 hr, incubated at 95°C in Laemmli sample buffer for 10 min, and analyzed on western blots. Images were captured using MicroChemi4.2 imaging system (DNR Bio-imaging Systems), and densitometry performed using GelQuant software (DNR Bio-imaging Systems). Background was subtracted using the rolling ball method, and densities were normalized to total H4 and expressed over one of the wild-type samples (equated to "1"). Antibodies are in Supplemental Experimental Procedures.

Behavioral Analyses

Mice were tested at 10 weeks of age, and their behavior was assessed as in Supplemental Experimental Procedures.

Statistics

All data other than the microarray were expressed as mean ± SEM and tested for significance with Student's t tests unless otherwise indicated, in which case they were analyzed with an ANOVA with Fisher's post hoc test or by two-way repeated-measures ANOVA (genotype X side) with Bonferroni's post hoc test.

SUPPLEMENTAL INFORMATION

Supplemental Information includes Supplemental Experimental Procedures, six figures, and two tables and can be found with this article online at http://dx.doi.org/10.1016/j.devcel.2014.11.031.

AUTHOR CONTRIBUTIONS

D.G. conceptualized and performed the phenotypic experiments, analyzed data, and cowrote the paper. A.V. conceptualized, performed, and analyzed the gene expression, histone acetylation, and ChIP experiments and cowrote the paper. M.A.Z. performed revisions and cowrote the paper. G.I.C. performed adult neurogenesis experiments. A.B. performed initial Ankrd11 expression studies. M.P.K. participated in gene expression analyses. C.A. performed behavioral analyses. M.T. cosupervised the behavioral studies. P.M.N. and D.F.C. provided antibodies and plasmids. S.W.S. provided intellectual input and unpublished data. G.M.K. supervised the human pluripotent cell work. K.W. supervised, conceptualized, and analyzed the behavioral experiments. D.R.K. and F.D.M. conceptualized and analyzed all experiments other than behavioral and cowrote the manuscript. All authors read and contributed to the manuscript.

ACKNOWLEDGMENTS

This work was funded by CIHR grant MOP-125945, a Brain Canada MIRI grant, and by the Three to Be Foundation. F.D.M. is an HHMI Senior International Research Scholar, and F.D.M. and D.R.K. are CRC chairholders. S.W.S. holds the GlaxoSmithKline-CIHR Chair in Genome Sciences. D.G. was funded by a McEwen Center McMurrich fellowship, A.V. by fellowships from the MS Society of Canada, CIHR, and Hospital for Sick Children, M.P.K. by a CIHR fellowship, and G.I.C. by a Heart and Stroke Foundation fellowship. We would particularly like to thank Martin Fray (MRC, Harwell) and the European Mutant Mouse Archive for help with the Yoda mice. We also thank Sarah Burns and Dennis Aquino for important technical assistance and Lisa Julian and Cheryl Arrowsmith for valuable advice.

Received: July 6, 2014
Revised: October 8, 2014
Accepted: November 20, 2014
Published: December 31, 2014

REFERENCES

Barbaric, I., Perry, M.J., Dear, T.N., Rodrigues Da Costa, A., Salopek, D., Marusic, A., Hough, T., Wells, S., Hunter, A.J., Cheeseman, M., and Brown, S.D.M. (2008). An ENU-induced mutation in the Ankrd11 gene results in an osteopenia-like phenotype in the mouse mutant Yoda. Physiol. Genomics *32*, 311–321.

Barnabé-Heider, F., Wasylnka, J.A., Fernandes, K.J., Porsche, C., Sendtner, M., Kaplan, D.R., and Miller, F.D. (2005). Evidence that embryonic neurons regulate the onset of cortical gliogenesis via cardiotrophin-1. Neuron *48*, 253–265.

Bowers, E.M., Yan, G., Mukherjee, C., Orry, A., Wang, L., Holbert, M.A., Crump, N.T., Hazzalin, C.A., Liszczak, G., Yuan, H., et al. (2010). Virtual ligand screening of the p300/CBP histone acetyltransferase: identification of a selective small molecule inhibitor. Chem. Biol. *17*, 471–482.

Cancino, G.I., Yiu, A.P., Fatt, M.P., Dugani, C.B., Flores, E.R., Frankland, P.W., Josselyn, S.A., Miller, F.D., and Kaplan, D.R. (2013). p63 Regulates adult neural precursor and newly born neuron survival to control hippocampal-dependent behavior. J. Neurosci. *33*, 12569–12585.

Carter, M.D., Shah, C.R., Muller, C.L., Crawley, J.N., Carneiro, A.M., and Veenstra-VanderWeele, J. (2011). Absence of preference for social novelty and increased grooming in integrin β3 knockout mice: initial studies and future directions. Autism Res. *4*, 57–67.

Castelo-Branco, G., Lilja, T., Wallenborg, K., Falcão, A.M., Marques, S.C., Gracias, A., Solum, D., Paap, R., Walfridsson, J., Teixeira, A.I., et al. (2014). Neural stem cell differentiation is dictated by distinct actions of nuclear receptor corepressors and histone deacetylases. Stem Cell Rep. *3*, 502–515.

Coles-Takabe, B.L., Brain, I., Purpura, K.A., Karpowicz, P., Zandstra, P.W., Morshead, C.M., and van der Kooy, D. (2008). Don't look: growing clonal versus nonclonal neural stem cell colonies. Stem Cells *26*, 2938–2944.

Crawley, J.N., Chen, T., Puri, A., Washburn, R., Sullivan, T.L., Hill, J.M., Young, N.B., Nadler, J.J., Moy, S.S., Young, L.J., et al. (2007). Social approach behaviors in oxytocin knockout mice: comparison of two independent lines tested in different laboratory environments. Neuropeptides *41*, 145–163.

Devlin, B., and Scherer, S.W. (2012). Genetic architecture in autism spectrum disorder. Curr. Opin. Genet. Dev. *22*, 229–237.

Gallagher, D., Norman, A.A., Woodard, C.L., Yang, G., Gauthier-Fisher, A., Fujitani, M., Vessey, J.P., Cancino, G.I., Sachewsky, N., Woltjen, K., et al. (2013). Transient maternal IL-6 mediates long-lasting changes in neural stem cell pools by deregulating an endogenous self-renewal pathway. Cell Stem Cell *13*, 564–576.

Iossifov, I., O'Roak, B.J., Sanders, S.J., Ronemus, M., Krumm, N., Levy, D., Stessman, H.A., Witherspoon, K.T., Vives, L., Patterson, K.E., et al. (2014). The contribution of de novo coding mutations to autism spectrum disorder. Nature *515*, 216–221, http://dx.doi.org/10.1038/nature13908.

Jamain, S., Radyushkin, K., Hammerschmidt, K., Granon, S., Boretius, S., Varoqueaux, F., Ramanantsoa, N., Gallego, J., Ronnenberg, A., Winter, D., et al. (2008). Reduced social interaction and ultrasonic communication in a mouse model of monogenic heritable autism. Proc. Natl. Acad. Sci. USA *105*, 1710–1715.

Li, C.W., Dinh, G.K., Zhang, A., and Chen, J.D. (2008). Ankyrin repeats-containing cofactors interact with ADA3 and modulate its co-activator function. Biochem. J. *413*, 349–357.

Lilja, T., Heldring, N., and Hermanson, O. (2013). Like a rolling histone: epigenetic regulation of neural stem cells and brain development by factors controlling histone acetylation and methylation. Biochim. Biophys. Acta *1830*, 2354–2360.

Lo-Castro, A., Brancati, F., Digilio, M.C., Garaci, F.G., Bollero, P., Alfieri, P., and Curatolo, P. (2013). Neurobehavioral phenotype observed in KBG syndrome caused by ANKRD11 mutations. Am. J. Med. Genet. B. Neuropsychiatr. Genet. *162B*, 17–23.

Marshall, C.R., Noor, A., Vincent, J.B., Lionel, A.C., Feuk, L., Skaug, J., Shago, M., Moessner, R., Pinto, D., Ren, Y., et al. (2008). Structural variation of chromosomes in autism spectrum disorder. Am. J. Hum. Genet. *82*, 477–488.

McCarthy, S.E., Gillis, J., Kramer, M., Lihm, J., Yoon, S., Berstein, Y., Mistry, M., Pavlidis, P., Solomon, R., Ghiban, E., et al. (2014). De novo mutations in schizophrenia implicate chromatin remodeling and support a genetic overlap with autism and intellectual disability. Mol. Psychiatry *19*, 652–658.

McQuown, S.C., Barrett, R.M., Matheos, D.P., Post, R.J., Rogge, G.A., Alenghat, T., Mullican, S.E., Jones, S., Rusche, J.R., Lazar, M.A., and Wood, M.A. (2011). HDAC3 is a critical negative regulator of long-term memory formation. J. Neurosci. *31*, 764–774.

Molina, J., Carmona-Mora, P., Chrast, J., Krall, P.M., Canales, C.P., Lupski, J.R., Reymond, A., and Walz, K. (2008). Abnormal social behaviors and altered gene expression rates in a mouse model for Potocki-Lupski syndrome. Hum. Mol. Genet. *17*, 2486–2495.

Moy, S.S., Nadler, J.J., Perez, A., Barbaro, R.P., Johns, J.M., Magnuson, T.R., Piven, J., and Crawley, J.N. (2004). Sociability and preference for social novelty in five inbred strains: an approach to assess autistic-like behavior in mice. Genes Brain Behav. *3*, 287–302.

Mullin, A.P., Gokhale, A., Moreno-De-Luca, A., Sanyal, S., Waddington, J.L., and Faundez, V. (2013). Neurodevelopmental disorders: mechanisms and boundary definitions from genomes, interactomes and proteomes. Transl. Psychiatr. *3*, e329.

Neilsen, P.M., Cheney, K.M., Li, C.W., Chen, J.D., Cawrse, J.E., Schulz, R.B., Powell, J.A., Kumar, R., and Callen, D.F. (2008). Identification of ANKRD11 as a p53 coactivator. J. Cell Sci. *121*, 3541–3552.

Pinto, D., Delaby, E., Merico, D., Barbosa, M., Merikangas, A., Klei, L., Thiruvahindrapuram, B., Xu, X., Ziman, R., Wang, Z., et al. (2014). Convergence of genes and cellular pathways dysregulated in autism spectrum disorders. Am. J. Hum. Genet. *94*, 677–694.

Rosenbloom, K.R., Sloan, C.A., Malladi, V.S., Dreszer, T.R., Learned, K., Kirkup, V.M., Wong, M.C., Maddren, M., Fang, R., Heitner, S.G., et al. (2013). ENCODE data in the UCSC Genome Browser: year 5 update. Nucleic Acids Res. *41*, D56–D63.

Rudenko, A., and Tsai, L.H. (2014). Epigenetic modifications in the nervous system and their impact upon cognitive impairments. Neuropharmacology *80*, 70–82.

Savage, J., Conley, A.J., Blais, A., and Skerjanc, I.S. (2009). SOX15 and SOX7 differentially regulate the myogenic program in P19 cells. Stem Cells *27*, 1231–1243.

Sirmaci, A., Spiliopoulos, M., Brancati, F., Powell, E., Duman, D., Abrams, A., Bademci, G., Agolini, E., Guo, S., Konuk, B., et al. (2011). Mutations in ANKRD11 cause KBG syndrome, characterized by intellectual disability, skeletal malformations, and macrodontia. Am. J. Hum. Genet. *89*, 289–294.

Söderberg, O., Gullberg, M., Jarvius, M., Ridderstråle, K., Leuchowius, K.J., Jarvius, J., Wester, K., Hydbring, P., Bahram, F., Larsson, L.G., and Landegren, U. (2006). Direct observation of individual endogenous protein complexes in situ by proximity ligation. Nat. Methods *3*, 995–1000.

Stoner, R., Chow, M.L., Boyle, M.P., Sunkin, S.M., Mouton, P.R., Roy, S., Wynshaw-Boris, A., Colamarino, S.A., Lein, E.S., and Courchesne, E. (2014). Patches of disorganization in the neocortex of children with autism. N. Engl. J. Med. *370*, 1209–1219.

Sun, G., Yu, R.T., Evans, R.M., and Shi, Y. (2007). Orphan nuclear receptor TLX recruits histone deacetylases to repress transcription and regulate neural stem cell proliferation. Proc. Natl. Acad. Sci. USA *104*, 15282–15287.

Tsui, D., Vessey, J.P., Tomita, H., Kaplan, D.R., and Miller, F.D. (2013). FoxP2 regulates neurogenesis during embryonic cortical development. J. Neurosci. *33*, 244–258.

Wang, J., Weaver, I.C., Gauthier-Fisher, A., Wang, H., He, L., Yeomans, J., Wondisford, F., Kaplan, D.R., and Miller, F.D. (2010). CBP histone acetyltransferase activity regulates embryonic neural differentiation in the normal and Rubinstein-Taybi syndrome brain. Dev. Cell *18*, 114–125.

Wang, J., Gallagher, D., DeVito, L.M., Cancino, G.I., Tsui, D., He, L., Keller, G.M., Frankland, P.W., Kaplan, D.R., and Miller, F.D. (2012). Metformin activates an atypical PKC-CBP pathway to promote neurogenesis and enhance spatial memory formation. Cell Stem Cell *11*, 23–35.

Willemsen, M.H., Fernandez, B.A., Bacino, C.A., Gerkes, E., de Brouwer, A.P., Pfundt, R., Sikkema-Raddatz, B., Scherer, S.W., Marshall, C.R., Potocki, L., et al. (2010). Identification of ANKRD11 and ZNF778 as candidate genes for autism and variable cognitive impairment in the novel 16q24.3 microdeletion syndrome. Eur. J. Hum. Genet. *18*, 429–435.

Yang, G., Smibert, C.A., Kaplan, D.R., and Miller, F.D. (2014). An eIF4E/4E-T complex determines the genesis of neurons from precursors by translationally repressing a proneurogenic transcription program. Neuron *84*, 723–739.

Zander, M.A., Burns, S.E., Yang, G., Kaplan, D.R., and Miller, F.D. (2014). Snail coordinately regulates downstream pathways to control multiple aspects of mammalian neural precursor development. J. Neurosci. *34*, 5164–5175.

Zhang, A., Yeung, P.L., Li, C.-W., Tsai, S.-C., Dinh, G.K., Wu, X., Li, H., and Chen, J.D. (2004). Identification of a novel family of ankyrin repeats containing cofactors for p160 nuclear receptor coactivators. J. Biol. Chem. *279*, 33799–33805.

Zhang, A., Li, C.-W., and Chen, J.D. (2007a). Characterization of transcriptional regulatory domains of ankyrin repeat cofactor-1. Biochem. Biophys. Res. Commun. *358*, 1034–1040.

Zhang, A., Li, C.W., Tsai, S.C., and Chen, J.D. (2007b). Subcellular localization of ankyrin repeats cofactor-1 regulates its corepressor activity. J. Cell. Biochem. *101*, 1301–1315.